J Mater Sci (2006) 41:7272–7278
DOI 10.1007/s10853-006-0142-4

Electrical properties and stability against DC accelerated aging stress of lanthania doped praseodymia-based zinc oxide varistor ceramics

Choon-Woo Nahm

Received: 16 November 2005 / Accepted: 31 March 2006 / Published online: 24 October 2006

Abstract The microstructure, electrical properties, and stability against DC accelerated aging stress of the varistor ceramics, which are composed of ZnO–Pr_6O_{11}–CoO–Cr_2O_3–La_2O_3-based ceramics, were investigated for various La_2O_3 contents. The increase of La_2O_3 content led to more densified ceramics, whereas abruptly decreased the nonlinear properties by incorporating beyond 1.0 mol%. The highest nonlinearity was obtained from 0.5 mol% La_2O_3, in which the nonlinear exponent is 81.6 and the leakage current is 0.1 μA. As the La_2O_3 content increased, the donor concentration increased in from 0.64×10^{18} to $16.89 \times 10^{18}/cm^3$ and the barrier height greatly decreased with increasing La_2O_3 content, reaching a maximum (1.47 eV) in 0.5 mol% La_2O_3. The varistors doped with 0.5 mol% La_2O_3 exhibited high stability, in which the variation rates of varistor voltage, nonlinear exponent, and leakage current were –1.14%, –3.7%, and +100%, respectively, for stressing state of 0.95 $V_{1\ mA}$/150 °C/24 h.

Introduction

Zinc oxide (ZnO) is oxide-semiconductor of nonstoichiometric defect structure that the zinc ion is more than oxygen ion. So, this is usefully used as material applying to gas sensor, devices using grain boundary effect, and so on. ZnO varistors are solid-state electronic devices manufactured by sintering a semiconducting ZnO grains with minor additives, such as Bi_2O_3, CoO, Cr_2O_3, and so on. ZnO varistors exhibit highly nonlinear conduction characteristics. In other words, ZnO varistors act as an insulator below the varistor voltage, called the breakdown voltage, and a conductor thereafter. Moreover, ZnO varistors possess excellent surge withstanding capability. Therefore, they have been widely applied to surge protection device (SPD), such as the surge absorbers in electronic systems and the surge arresters in electric power systems [1, 2].

Their electrical characteristics are related to a unit structure composed of ZnO grain-intergranular layer-ZnO grain in the bulk of the devices. A unit structure acts as if it has a semiconductor junction at grain boundary. Since the nonlinear electrical behavior occurs at a boundary of each semiconducting ZnO grain, the varistor ceramics can be considered a multi-junction device composed of many series and parallel connection of grain boundary. The grain size distribution plays a major rule in electrical behavior.

Many researchers who are interested in the varistor ceramics commonly wish to fabricate ZnO varistor ceramics with a higher nonlinearity. The majority of commercial varistor ceramics are Bi_2O_3-based ZnO varistor ceramics containing Bi_2O_3, which inherently induces nonlinear properties. Recently, Pr_6O_{11}-based ZnO varistor ceramics have been studied in order to improve a few drawbacks [3] due to the high volatility and reactivity of Bi_2O_3 [4–17]. Nahm et al. reported that ZnO–Pr_6O_{11}–CoO–Cr_2O_3-based varistor ceramics have highly nonlinear properties when rare-earth metal oxides, R_2O_3 (R = Er, Y, Dy) are used [9–17].

C.-W. Nahm (✉)
Department of Electrical Engineering, Dongeui University, Busan 614-714, Korea
e-mail: cwnahm@deu.ac.kr

This paper is to investigate the effect of La_2O_3 on microstructure, nonlinear properties, capacitance–voltage characteristics, dielectric characteristics, and stability of ZnO–Pr_6O_{11}–CoO–Cr_2O_3–La_2O_3-based varistor ceramics.

Experimental procedure

Sample preparation

Reagent-grade raw materials were prepared for varistor ceramics with a composition expression, such as (98.0-x) mol% ZnO, 0.5 mol% Pr_6O_{11}, 1.0 mol% CoO, 0.5 mol% Cr_2O_3, x mol% La_2O_3 (x = 0.0, 0.5, 1.0, 2.0). Raw materials were mixed by ball milling with zirconia balls and acetone in a polypropylene bottle for 24 h. The mixture was dried at 120 °C for 12 h and calcined in air at 750 °C for 2 h. The calcined mixture was pulverized using an agate mortar/pestle and after 2 wt% polyvinyl alcohol (PVA) binder addition, granulated by sieving through a 100-mesh screen to produce the starting power. The power was uniaxially pressed into discs of 10 mm in diameter and 2 mm in thickness at a pressure of 80 MPa. The discs were placed in the starting power using an alumina crucible, sintered at 1,300 °C in air for 1 h, and furnace-cooled to room temperature. The heating and cooling rates were 4 °C/min. The sintered samples were lapped and polished to 1.0 mm thickness. The size of the final samples was about 8 mm in diameter and 1.0 mm in thickness. Silver paste was coated on both faces of samples and the silver electrodes were formed by heating at 600 °C for 10 min. The electrodes were 5 mm in diameter.

Microstructure measurement

Either surface of samples was lapped and ground with SiC paper and polished with 0.3 μm-Al_2O_3 powder to a mirror-like surface. The polished samples were thermally etched at 1,100 °C for 30 min. The surface microstructure was examined by a scanning electron microscope (SEM, Hitachi S2400, Japan). The average grain size (d) was determined by the lineal intercept method such the following equation [18].

$$d = \frac{1.56L}{MN} \tag{1}$$

where L is the random line length on the micrograph, M is the magnification of the micrograph, and N is the number of the grain boundaries intercepted by lines [18]. The compositional analysis of the selected areas was determined by an attached energy dispersion X-ray analysis (EDX) system. The crystalline phases were identified by an X-ray diffractometry (XRD, Rigaku D/max 2100, Japan) using a CuK_α radiation. The density (ρ) of varistor ceramics was measured by the Archimedes method.

Electrical measurement

The current–voltage (I–V) characteristics of varistor ceramics were measured using a V–I source/measure unit (Keithley 237). The varistor voltage ($V_{1\ \mathrm{mA}}$) was measured at 1.0 mA/cm^2 and the leakage current (I_L) was defined as the current at 0.80 $V_{1\ \mathrm{mA}}$. In addition, the nonlinear exponent (α) is defined by the following equation.

$$\alpha = \frac{\log J_2 - \log J_1}{\log E_2 - \log E_1} \tag{2}$$

where E_1 and E_2 are the electric fields corresponding to J_1 = 1.0 mA/cm^2 and J_2 = 10 mA/cm^2, respectively.

The capacitance–voltage (C–V) characteristics of varistor ceramics were measured at 1 kHz and 1 V_{rms} using a RLC meter (QuadTech 7600) and an electrometer (Keithley 617). The donor concentration (N_d) of ZnO grains and the barrier height (ϕ_b) at the grain boundary were determined from the slope and intercept of straight line, respectively, using the following equation proposed by Mukae et al. [19].

$$\left(\frac{1}{C_b} - \frac{1}{2C_{bo}}\right)^2 = \frac{2(\phi_b + V_{gb})}{q\varepsilon N_d} \tag{3}$$

where C_b is the capacitance per unit area of a grain boundary, C_{bo} is the value of C_b when V_{gb} = 0, V_{gb} is the applied voltage per grain boundary, q is the electronic charge, and ε is the permittivity of ZnO ($\varepsilon = 8.5\varepsilon_o$). The density of interface states (N_t) at the grain boundary was determined by the following equation [19] using the value of the donor concentration and barrier height obtained above.

$$N_t = \left(\frac{2\varepsilon N_d \phi_b}{q}\right)^{1/2} \tag{4}$$

Once the donor concentration and barrier height are known, the depletion layer width (t) of either side at the grain boundaries was determined by the following equation [20].

$$N_d\, t = N_t \tag{5}$$

The dielectric characteristics, such as the apparent dielectric constant (ε_{APP}') and dissipation factor ($\tan\delta$), were measured in the range of 100 Hz–2 MHz using a RLC meter (QuadTech 7600).

DC-accelerated aging characteristic measurement

The stability against DC accelerated aging stress were performed for the four continuous states; (i) 1st stress: 0.85 $V_{1\,mA}$/115 °C/24 h, (ii) 2nd stress: 0.90 $V_{1\,mA}$/120 °C/24 h, (iii) 3rd stress: 0.95 $V_{1\,mA}$/125 °C /24 h, and (iv) 4th stress: 0.95 $V_{1\,mA}$/150 °C/24 h. Simultaneously, the leakage current during the stress time was monitored at intervals of 1 min by a high voltage source-measure unit (Keithley 237). The electrical characteristics for varistors stressed were performed after storage at normal room temperature for 2 h. The degradation rate coefficient (K_T) was calculated from the following equation [21].

$$I_L = I_{Lo} + K_T t^{1/2} \tag{6}$$

where I_L is the leakage current at stress time (t) and I_{Lo} is I_L at $t = 0$. After the respective stresses, the V–I and dielectric characteristics were measured at room temperature. In treatment of numerical data, 5 samples varistor ceramics sintered at the same composition were used in all electrical measurements and their average value was used.

Results and discussion

Figure 1 shows the SEM micrographs of varistor ceramics with various La_2O_3 contents. It is well known that the microstructure of Pr_6O_{11}-based ZnO varistor ceramics is consisted of only two phases [22]: ZnO grain (bulk phase) and intergranular layer (second phase). The intergranular layers in varistor ceramics were Pr- and La-rich phases as determined by XRD analysis, as shown in Fig. 2. As can be seen in the figure, three diffraction peaks were revealed in varistor ceramics, namely, ZnO grains, Pr oxides, and La_2O_3 oxide. It was found from that these coexist at the grain boundaries and the nodal points as if they were a single phase, as shown in the EDAX analysis in Fig. 3. No La peak was found in the ZnO grain within the EDX detection limit. It was observed by SEM that as the La_2O_3 content increased, the intergranular phase gradually becomes more concentrated at the nodal points. It is assumed that this is attributed to the segregation of La toward grain boundaries due to the difference of ionic radius. These microstructures are not greatly different with varistor ceramics doped with Er, Y, and Dy, as reported previously [9, 12, 16]. As the La_2O_3 content increased, the density increased from 4.71 g/cm^3 to 5.77 g/cm^3 up to 1.0 mol%, whereas the further addition did not affect density, which saturated at 5.77 g/cm^3. La_2O_3 seems to severe as an adder related to liquid phase sintering. The average grain size increased from 4.0 μm to 8.5 μm with increasing La_2O_3 content due to precipitation of Pr_6O_{11} and La_2O_3 at

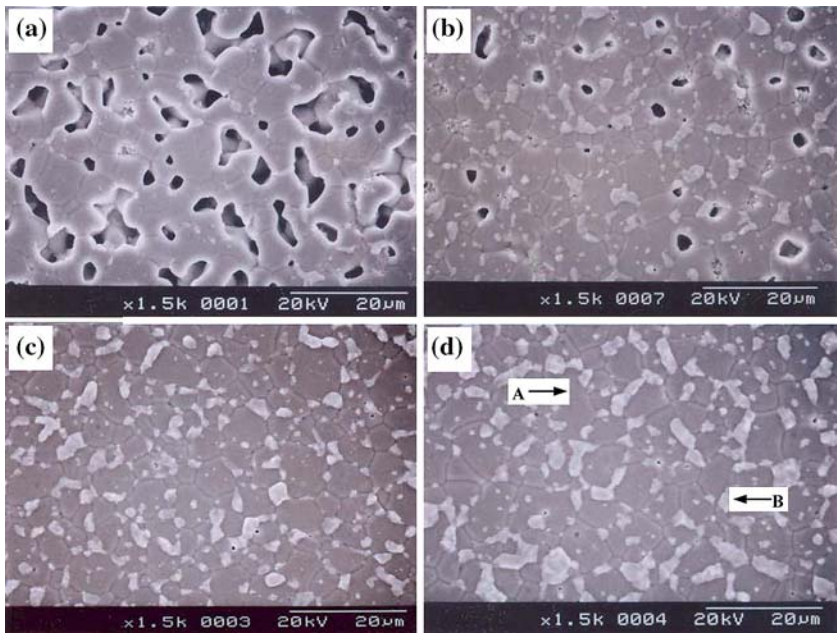

Fig. 1 SEM micrographs of varistor ceramics with various La_2O_3 contents; (**a**) 0.0 mol%, (**b**) 0.5 mol%, (**c**) 1.0 mol%, and (**d**) 2.0 mol% (A: ZnO grain and B: intregranular layer)

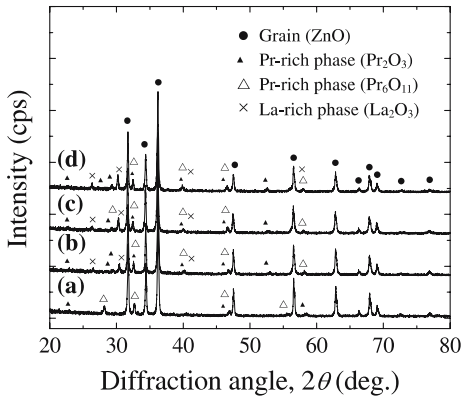

Fig. 2 XRD patterns of varistor ceramics with various La_2O_3 contents; (**a**) 0.0 mol%, (**b**) 0.5 mol%, (**c**) 1.0 mol%, and (**d**) 2.0 mol%

grain boundaries. The tendency of decrease in the average grain size directly affects the varistor voltage in the electrical properties. The detailed microstructual parameters are summarized in Table 1.

Figure 4 shows the *E–J* characteristics of varistor ceramics with various La_2O_3 contents. The conduction characteristics of varistor ceramics are divided into two regions: pre-breakdown at low field and breakdown at high field. The sharper the knee of the curves between the two regions, the better the nonlinearity. It can be forecasted that the varistor ceramics doped with 0.5 mol% La_2O_3 would exhibit the best nonlinear properties because it has the sharpest knee. As adding more La_2O_3, the knee gradually becomes less pronounced and the nonlinear properties reduce. The detailed *V–I* characteristic parameters are summarized in Table 1. The varistor voltage ($V_{1\,mA}$) decreased abruptly from 503.5 V/mm to 9.4 V/mm as the La_2O_3 content increased. This is attributed firstly to the decrease in the number of grain boundaries caused by the increase in the ZnO grain size, and secondly, to the abrupt decrease of varistor voltage per grain boundaries (V_{gb}). The varistors doped with La_2O_3 exceeding 0.5 mol% exhibited much lower V_{gb} value than general value of 2–3 V/gb. These varistors will exhibit very poor nonlinear properties presumably. The varistor voltage per grain boundaries (V_{gb}) is defined by the following equation.

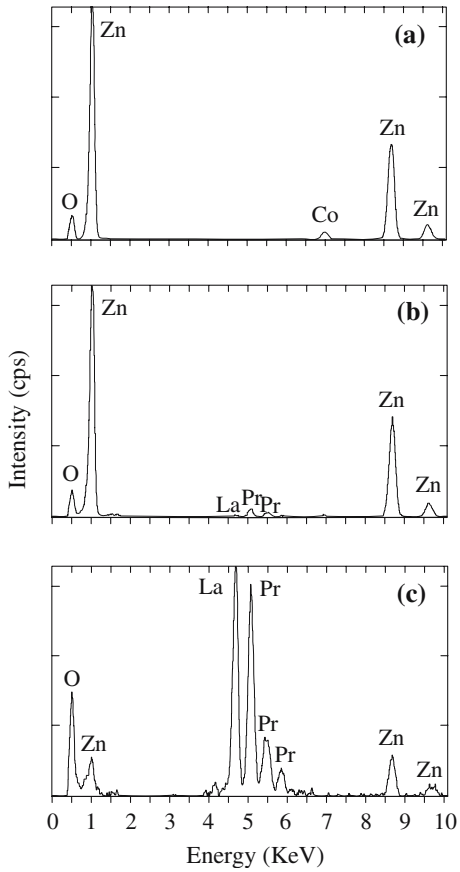

Fig. 3 EDX analysis of varistor ceramics with 0.5 mol% La_2O_3 content; (**a**) ZnO grain, (**b**) Grain boundary, and (**c**) Intergranular layer

$$V_{gb} = \left(\frac{d}{D}\right) V_{1\,mA} \tag{7}$$

where d is the average grain size and D is thickness of sample.

The nonlinear exponent (α) value was calculated to be 63.0 in the case of varistor ceramics without La_2O_3. This value was much higher than that of the quaternary system $ZnO–Bi_2O_3–CoO–Cr_2O_3$-based ceramics, which never exceeded 25. As the La_2O_3 content increased, the α value increased, achieving a maximum value (81.6) for varistor ceramics with 0.5 mol% La_2O_3. This value is easily unobtainable excellent nonlinearity in ZnO varistor ceramics. This is the

Table 1 Microstrucrural, *V–I*, *C–V*, and dielectric parameters of varistor ceramics with various La_2O_3 contents

La_2O_3 content (mol%)	ρ (g/cm^3)	d (μm)	$V_{1\,mA}$ (V/mm)	V_{gb} (V/gb)	α	I_L (μA)	N_d (10^{18}/cm^3)	N_t (10^{12}/cm^2)	ϕ_b (eV)	t (nm)	ε_{APP}'	tanδ
0.0	4.71	4.0	503.5	2.0	63.0	2.1	0.64	2.21	0.82	34.6	484.7	0.0772
0.5	5.40	6.9	427.2	2.9	81.6	0.2	0.94	3.60	1.47	38.4	737.9	0.0784
1.0	5.77	7.9	108.0	0.8	7.1	50.6	2.59	4.04	0.67	15.6	2129.5	0.2839
2.0	5.77	8.5	9.4	0.08	3.1	100.2	16.89	5.16	0.17	3.1	11911.5	0.6003

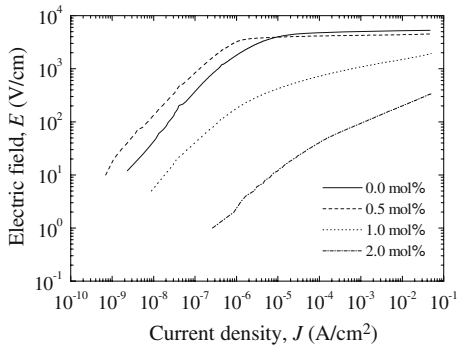

Fig. 4 *E–J* characteristics of varistor ceramics with various La_2O_3 contents

highest value in Pr_6O_{11}-based ZnO varistor ceramics of five-components that has been achieved. Increasing La_2O_3 content further to 2.0 mol% caused the α value (3.1) to decrease. On the other hand, as the La_2O_3 content increased, the leakage current (I_L) value decreased, achieving a minimum value (0.2 μA) for the varistor ceramics with 0.5 mol% La_2O_3. Increasing La_2O_3 content further to 2.0 mol% caused the I_L value (100.2 μA) to increase significantly. It can be seen that the variation of I_L shows the inverse relationship to the variation of α with La_2O_3 content. As a result, it is clear that the nonlinear properties are strongly influenced by the incorporation of La_2O_3. The reason why 0.5 mol% La_2O_3 exhibits the highest nonlinearity is attributed to the highest barrier height, which will be referred in *C–V* characteristics.

Figure 5 shows *C–V* characteristics of varistor ceramics with various La_2O_3 contents. The detailed *C–V* characteristic parameters are summarized in Table 1. The N_d value increased abruptly monotonously in the range of 0.64×10^{18}–$16.89 \times 10^{18}/cm^3$ with increasing La_2O_3 content. This means the La_2O_3 acts as donor. Although La^{3+} ions have a larger radius (0.106 nm) than Zn^{2+} ions (0.074 nm), limited substitution within the ZnO grains is possible. La substitutes

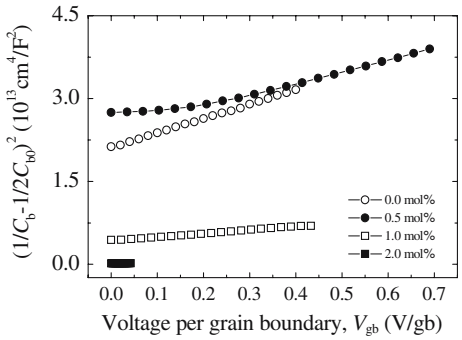

Fig. 5 *C–V* characteristics of varistor ceramics with various La_2O_3 contents

for Zn and creates lattice defect in ZnO grains. The chemical-defect reaction using *kröger – vink* notation can be written as the following equation.

$$La_2O_3 \xrightarrow{ZnO} 2La^{\bullet}_{Zn} + 3O^{\times}_{O} + 2e' \quad (8)$$

where $La^{\bullet}_{Zn}$ is a positively charged La ion substituted for Zn lattice site and $O^{\times}_{O}$ is a neutral oxygen of oxygen lattice site. The electron generated in reaction above increases the donor concentration. The t value on either side of depletion region decreased in the range of t = 34.6–3.1 nm with increasing La_2O_3 content. This shows opposite relation to the N_d. In general, the depletion region extends farther into the side with a lighter doping. On the other hand, the increase of La_2O_3 content led to the increase in the N_t value in the range of 2.21×10^{12}–$5.16 \times 10^{12}/cm^2$. The ϕ_b value decreased in the range of 1.4–0.17 eV with increasing La_2O_3 content, reaching a maximum (1.47 eV) in 0.5 mol% La_2O_3. This coincides with the variation of α value in *V–I* characteristics. The ϕ_b is directly associated with the N_d and N_t. In other words, the ϕ_b is estimated by the variation rate in the N_t and N_d. In general, the ϕ_b is increased with increasing N_t and decreasing N_d.

Figure 6 shows the frequency dependence of dielectric characteristics of varistor ceramics with various La_2O_3 contents. The apparent dielectric constant

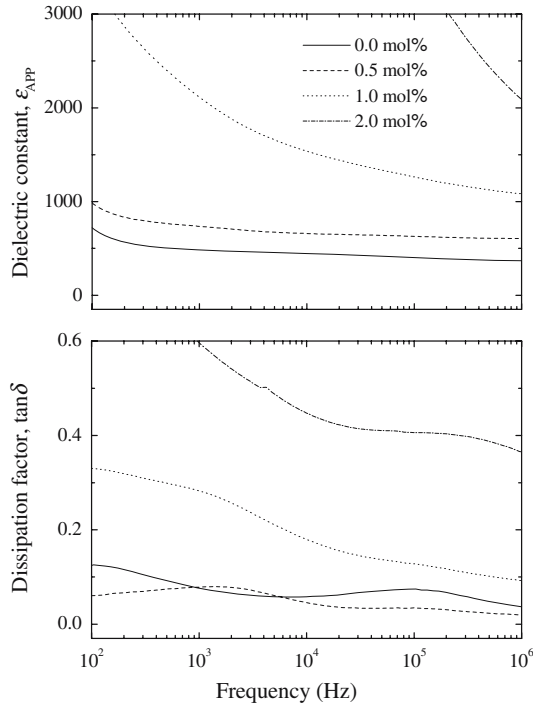

Fig. 6 Frequency dependence of dielectric characteristics of varistor ceramics with various La_2O_3 contents

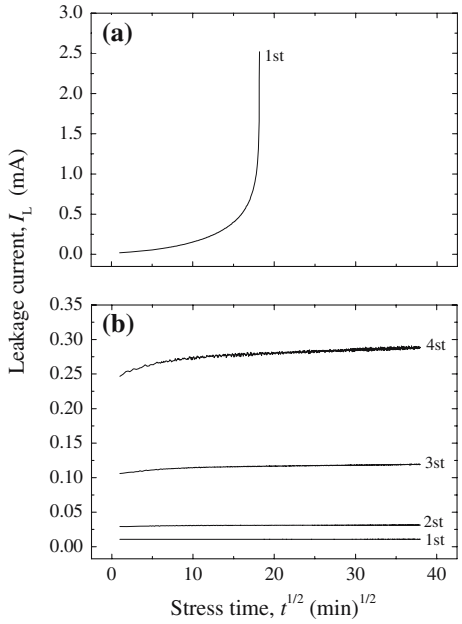

Fig. 7 Variation of leakage current during DC accelerated aging stress of varistor ceramics doped with La_2O_3; (**a**) 0.0 mol% and (**b**) 0.5 mol%

(ε_{APP}') decreased gradually without a sharper dispersive drop being evident as the frequency increased, which is associated with the polarization of dielectrics. The apparent dielectric constant in the measuring frequency range increased with increasing La_2O_3 content. This is directly related to the average grain size, as can be seen in the following equation.

$$\varepsilon_{APP}\prime = \left(\frac{d}{t}\right)\varepsilon_g \tag{9}$$

where ε_g is the dielectric constant of ZnO, d is the average grain size, and t is the depletion layer width. It can be seen that the larger grain in comparison gives rise to a higher ε_{APP}' value. The detailed dielectric parameters at 1 kHz are summarized in Table 1. It was found that the values of dissipation factor (tanδ) are very greatly affected by La_2O_3 content and on the whole, very complex. The tanδ of varistor ceramics except for La_2O_3 content of 0.5 mol% exhibited to be very high more than 10% at 1 kHz. Although the varistor ceramics with 0.5 mol% La_2O_3 have low leakage current, the tanδ is high compared with other rare-earth metal oxides such as Er_2O_3, Y_2O_3, and Dy_2O_3 less than 5% in tanδ. The tanδ is composed of joule heating loss by leakage current and friction heating loss by electric dipole rotation. It is assumed that the reason why they possess high tanδ is because they are more greatly affected by the former than the latter.

Figure 7 shows the variation of leakage current during various DC accelerated aging stresses of varistor ceramics doped with 0.0 and 0.5 mol% La_2O_3, which have only high nonlinearity. The ZPCC-based varistor ceramics doped without La_2O_3 exhibited a thermal runaway under the first stress, even under relatively weak stress, exhibited the thermal runaway within short time. Although this varistor possesses a good nonlinearity, to be easily degraded is attributed to the low density, which decreases the number of conduction path and eventually leads to the concentration of current. On the other hand, the varistor ceramics doped with 0.5 mol% La_2O_3 show high stability without thermal runaway until the 4th stress. It can be seen that the leakage current was nearly constant (K_T = 0.24–0.25 $\mu A{\cdot}h^{-1/2}$) until the 2nd stress, but weak positive creep of leakage current (K_T =1.48 – 1.50 $\mu A{\cdot}h^{-1/2}$) under the 3rd stress and remarkable creep (K_T =4.65 – 4.68 $\mu A{\cdot}h^{-1/2}$) during the 4th stress. It is assumed that this high stability is attributed to the density higher and the leakage current lower. The variations of *V–I* and dielectric characteristic parameters after various DC stresses in varistor ceramics doped with 0.5 mol% La_2O_3 are summarized in Table 2.

These varistor ceramics exhibited high stability for *V–I* characteristics, in which the variation rate of varistor voltage ($\%\Delta V_{1\,mA}$) is –1.14%, of nonlinear exponent ($\%\Delta\alpha$) is –3.7%, and of leakage current ($\%\Delta I_L$) is +100% after the 4th stress. The leakage current greatly changed compared with initial value after the 4th stress, whereas only 0.4 μA. On the

Table 2 Variation rate of *V–I* and dielectric parameters of after DC accelerated aging stress of varistor ceramics doped with 0.5 mol% La_2O_3

Stress state	$V_{1\,mA}$ (V/mm)	$\%\Delta V_{1\,mA}$	α	$\%\Delta\alpha$	I_L (μA)	$\%\Delta I_L$	ε_{APP}'	$\%\Delta\varepsilon_{APP}'$	tanδ	$\%\Delta$tanδ
Before	427.2	0	81.6	0	0.2	0	737.9	0	0.0784	0
1st	424.7	–0.59	81.2	–0.5	0.1	–50	735.7	–0.3	0.0768	–2.0
2nd	424.0	–0.75	80.1	–1.8	0.1	–50	740.6	0.4	0.0770	–1.8
3rd	423.2	–0.94	78.1	–4.3	0.2	0	741.4	0.5	0.0785	0.1
4th	422.3	–1.14	78.6	–3.7	0.4	100	748.4	1.4	0.0848	8.2

other hand, the stability for dielectric characteristics exhibited a high stability, with +1.4% in the variation rate of dielectric constant ($\%\Delta\varepsilon_{APP}'$) and +8.2% in the variation rate of dissipation factor ($\%\Delta\tan\delta$).

Conclusions

The microstructure, electrical properties, dielectric characteristics, and stability of varistor ceramics were investigated for various La_2O_3 contents. The ceramics were more densified in the range of 4.71–5.77 g/cm^3 with increasing La_2O_3 content. The varistor voltage decreased abruptly in the range of 503.5–9.4 V/mm with increasing La_2O_3 content. It was found that a moderate La_2O_3 content, in the vicinity of 0.5 mol%, could greatly improve the nonlinear properties of quaternary system ZnO–Pr_6O_{11}–CoO–Cr_2O_3-based varistor ceramics. The varistor ceramics with 0.5 mol% La_2O_3 exhibited excellent nonlinear properties, in which the nonlinear exponent is 81.6 and the leakage current is 0.2 μA. The La_2O_3 was additives acting as a donor by increasing donor concentration with increasing La_2O_3 content. The varistor ceramics doped with 0.5 mol% La_2O_3 also exhibited high stability, with the variation rate of varistors voltage of –1.14%, of nonlinear exponent of –3.7%, of leakage current of +100%, of dielectric constant of +1.4%, and of dissipation factor of +8.2% for stressing state of 0.95 $V_{1\ mA}$/150 °C/24 h. Remainder varistor ceramics doped with La_2O_3 exhibited considerably poor nonlinearity.

References

1. Levinson LM, Pilipp HR (1986) Amer Ceram Soc Bull 65:639
2. Gupta TK (1990) J Amer Ceram Soc 73:1817
3. Lee YS, Tseng TY (1992) J Amer Ceram Soc 75:1636
4. Alles AB, Burdick VL (1991) J Appl Phys 70:6883
5. Alles AB, Puskas R, Callahan G, Burdick VL (1993) J Am Ceram Soc 76:2098
6. Lee Y-S, Liao K-S, Tseng T-Y (1996) J Amer Ceram Soc 79:2379
7. Wakiya N, Chun SY, Lee CH, Sakurai O, Shinozaki K, Mizutani N (1999) J Electroceram 4(S1):15
8. Chun SY Mizutani N (2001) Mater Sci Eng B79:1
9. Nahm C-W (2001) Mater Lett 47:182
10. Nahm C-W (2002) Mater Lett 53:110
11. Nahm C-W (2003) J Europ Ceram Soc 23:1345
12. Nahm C-W (2003) Mater Lett 57:1317
13. Nahm C-W (2003) Mater Lett 57:1322
14. Nahm C-W, Shin B-C (2004) Ceram Int 30:9
15. Nahm C-W (2003) Solid State Commun 127:389
16. Nahm C-W (2004) Mater Lett 58:2252
17. Nahm C-W (2004) Mater Lett 58:3297
18. Wurst JC, Nelson JA (1972) J Am Ceram Soc 55:109
19. Mukae M, Tsuda K, Nagasawa I (1979) J Appl Phys 50:4475
20. Hozer L (1994) Semiconductor ceramics: grain boundary effects. Ellis Horwood, p 22
21. Fan J, Freer R (1994) J Amer Cearm Soc 77:2663
22. Mukae K (1987) Am Ceram Soc Bull 66:1329